Wavelet diagnostics for detection of coherent structures in instantaneous turbulent flow imagery: A review

RODDAM NARASIMHA

Jawaharlal Nehru Centre for Advanced Scientific Research, Bangalore 560 064
e-mail: {roddam@caos.iisc.ernet.in}

Abstract.   A review of work over the last decade shows that 2D wavelet techniques applied on flow imagery can provide powerful insights into the nature and life-cycle of coherent structures (the latter through wavelet movies) in turbulent shear flows. The advantage of wavelet techniques in often being able to infer the nature of coherent motion from a single image is emphasized. The techniques are first calibrated by using them on well-known results in the turbulent mixing layer. They are then applied to jets and plumes, and it is shown how off-source heating in such flows can disrupt the coherent structures in the unheated flow. A suitably reduced version of the present method, using discrete wavelet transforms on signals from a finite array of sensors, could be a useful diagnostic tool in near-real-time detection of coherent structures or patterns for the purpose of selecting appropriate control signals to the actuators in a flow-control system.

Keywords.   Turbulent flow imagery; 2D wavelet techniques; coherent structures; flow-control system.

1. Introduction

Active control of turbulent flow usually involves manipulating, in real time, any coherent structure present in the flow to be controlled. An effective control system has to perform the following functions:

- sense the flow at sufficiently frequent intervals at each of an array of sites;
- detect from the sensor output any structure present in the flow that can be manipulated so as to achieve the design goals set for the control system;
- based on the detected structure or pattern, and an appropriate algorithm, make a decision regarding whether (and if so, where and how) control has to be applied for achieving the best results; and
- operate a suitable actuator to feed the control signal into the flow in accordance with the decision.

The present work chiefly concerns the first two steps, namely a method of detecting structure from the outputs of a suitable array of sensors, each of which generates a time series. The problem addressed is the one of inferring the type and intensity of any spatial structures

present in the flow from sensor output, and their stage in the life-cycle of the structure. The actual problem tackled is the somewhat wider one of analysing instantaneous flow imagery in order to detect any underlying structure. Flow imagery may often consist of pixels, numbering in the order of a million. In any specific control application, the number of sensor outputs to be processed may be appreciably smaller, but in principle the nature of the problem in both cases is the same, namely that of separating order from disorder in the sensor output.

The present paper is a review of wavelet-based techniques for the eduction of coherent structures from flow imagery. Such techniques have several potential applications. Apart from possible use in active control systems, they can also suggest the most effective locations and variables for the operation of the actuator, and in a more fundamental way help illuminate the dynamics of the (uncontrolled) flow itself. We will review the methods we have developed and our experience with them over the last decade.

Section 2 reviews coherent structures and §3 briefly describes wavelets and the method we adopt. Section 4 calibrates the method with the well-known results of turbulent flow in a mixing layer. Section 5 describes results with jet and plume flow, studied with and without injection of off-source heating; the original motivation here was to test certain ideas providing an explanation for the anomalous entrainment characteristics of clouds, simulating their fluid dynamics by the injection of dynamically similar quantities of heat into a laboratory flow. Section 6 summarises the present state of the technique.

2. Coherent structures

The first dramatic evidence of coherent structures in a fully developed turbulent shear flow came from the visualization studies of Roshko and his co-workers (e.g. Brown & Roshko 1974; Roshko 1976) in mixing layers, using schlieren and shadowgraph pictures, and of Kline *et al* (1967) in a boundary layer, using the hydrogen-bubble technique. It became clear that despite its apparent disorder, a turbulent shear flow may possess considerable order, to a greater or lesser degree depending on the flow. More quantitative studies have used two-point space–time correlations of velocity fluctuations (Tso & Hussain 1989). However, the averaging process inherent in the correlation technique may underestimate the degree of order present, especially as there is considerable jitter in the structures, and both temporal and spatial scales can be highly variable. When there are several types of structure with different scales, such techniques cannot reveal whether their occurrence is simultaneous or not. Reviews of early work are provided by Hussain (1986) and Fiedler (1988).

With the advent of digital imagery, more advanced experimental techniques such as laser-induced fluorescence, particle and holographic imaging velocimetry, high-resolution direct numerical simulations, and novel image-processing techniques, it is becoming feasible to obtain more quantitative information on coherent structures than ever before. The simplest image processing technique involves thresholding and averaging (e.g. Cutler & Johnson 1997). A more powerful tool is the wavelet transform. The present review describes the state of the art in the use of the wavelet techniques as developed and applied with a group of colleagues and students at the Indian Institute of Science and the Jawaharlal Nehru Centre for Advanced Scientific Research in Bangalore (Kailas & Narasimha 1999; Siddhartha *et al* 2000; Narasimha *et al* 2002; Srinivas *et al* 2007).
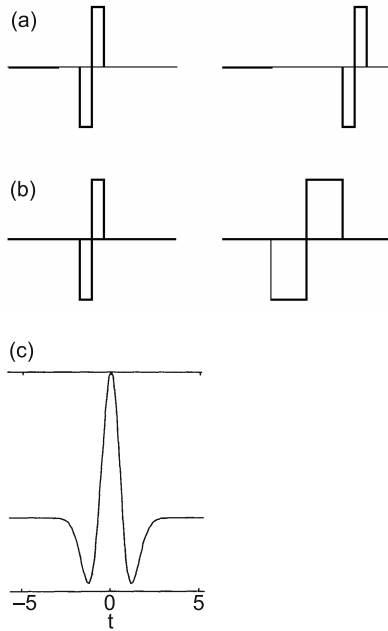
(a)

(b)

(c)

−5   0   5
t

Figure 1. **(a)** and **(b)** illustrate respectively the translation and dilation of Haar wavelets, which are simple pairs of rectangular pulses of opposite sign; (a) illustrates translation of the wavelet along the *t* axis, (b) illustrates dilation, namely the increase in the scale *a*. **(c)** The form of a one-dimensional Mexican-hat wavelet.

3. The wavelet technique

The wavelet transform $\hat{f}(\boldsymbol{x}, a)$ of a function $f(\boldsymbol{x})$ may be defined as the convolution product of a scaled and shifted mother wavelet $\psi(\boldsymbol{x})$ with the function to be analysed:

$$\hat{f}(\boldsymbol{x}, a) = \int f(\boldsymbol{x}')\psi[(\boldsymbol{x} - \boldsymbol{x}')/a]\mathrm{d}\boldsymbol{x}', \tag{1}$$

where a is the so-called scale parameter and $\boldsymbol{x}'$ the shift parameter (figure 1). Note that the transform is defined at each value of $\boldsymbol{x}$: the transform may be seen as a rigorous and mathematically attractive way of performing a variable-scale weighted moving average. Detailed reviews of wavelet-transform principles and techniques are available in Strang (1989) and Meyer (1993); an accessible introduction describing many applications is given by Addison (2002). Briefly, the mother wavelet must be a rapidly decaying function of its argument (i.e. must have compact support), have a zero mean, and possess a Fourier transform that has a special integrability property; these conditions ensure invertibility and preservation of the L^2 norm. Several such functions exist in the wavelet literature. Results do depend on the choice of wavelet (Arneodo *et al* 1996; Azad & Narasimha 2007), and some effort may be needed to find the best choice in a particular application (e.g. see the latter reference, which considers the problem of detecting periodicities in rainfall data).

In our work we have used the continuous version of the transform as in (1), which is redundant but provides complete freedom in the choice of wavelet scale. The transform is particularly useful because of its power as a filter that can help detect ordered structures at different scales in an instantaneous visualization of the flow. In real-life applications in flow control, the discrete wavelet transform operating on outputs from a finite array of sensors is more likely to be appropriate.

Early work on the use of wavelets to study coherent structures includes most notably Farge (1992), who reconstructed scale-specific regions of high vorticity concentration in direct numerical simulations by inverting the wavelet transform, and used it to study the dynamics of these structures.

In the present case, our purpose is to detect structures at various spatial scales. We have found it convenient to use the two-dimensional Mexican-hat wavelet for this purpose:

$$\psi(x) = (2 - x^2 - y^2) \exp{-(x^2 + y^2)/2},$$

where $\boldsymbol{x} \equiv (x, y)$ is the two-dimensional position vector in the plane of the image being analysed, with x and y being appropriate Cartesian coordinates. The zero-crossings of this transform have been shown to be particularly useful in detecting regions of sharp gradients in an image (Marr 1982). Such gradients may assist in identifying the interfaces between the more- and less-mixed flow regions, and between coherent and non-coherent motion.

We usually replace the scale a of the wavelet transform by a', which is non-dimensionalized by some characteristic length L of the image. Since the wavelet transform at the smallest scales is sensitive to the fine scale noise occurring on an otherwise smooth background, it is necessary to remove the (almost unnoticeable) digitisation noise from the background representing ambient flow. After trying various quantitative methods to remove this noise, Kailas & Narasimha (1999) found the following procedure effective. The raw image is first carefully trimmed to retain all of the relevant flow field, and the background is uniformly set to the average pixel intensity towards the edge of the flow bordering the background. There is no visually discernible difference between this version and the original image, except that the small-scale background noise is completely eliminated. Some thresholding within the flow as well may be required at the smaller scales to remove noise. At the larger scales, no thresholding is necessary. Some additional refinements found to be useful are described in Kailas & Narasimha (1999).

4. The mixing layer

To calibrate the techniques we adopt, the mixing layer – in both laminar and turbulent states – was first studied using wavelet transforms by Kailas & Narasimha (1999). They analysed the flow visualizations of a mixing layer by Brown & Roshko (1974); the main results are shown in figures 2 and 3 and discussed briefly below.

Figure 2 shows the wavelet transforms of the turbulent mixing layer at seven different wavelet scales increasing dyadically from $a' = 0.01$ (the non-dimensionalizing scale L is the streamwise length of the field of view in the figures). It is interesting that at the lowest two wavelet scales ($a' = 0.01$ and 0.02) the whole mixing layer appears to be covered by a nearly homogeneous distribution of very fine scale structures. These, at first glance, appear to be of approximately the same size over the whole domain of observation: there is actually a slow variation, as we shall see shortly. On the other hand, Everson *et al* (1990), studying dye concentration in longitudinal sections of a jet illuminated by a laser sheet, note that the size of the small-scale structures in the jet increases with downstream distance from the exit nozzle. Part of the reason for this observation is that the two flows have different structure; we must also remember that in the present case the imagery being analysed is *not* a section of the flow but (being obtained from a spank shadowgraph) represents in some sense a spanwise integral across the flow.

With increasing wavelet scale, the connectedness among the structures is more clearly manifested and an intermediate scale structure of the mixing layer becomes apparent. At
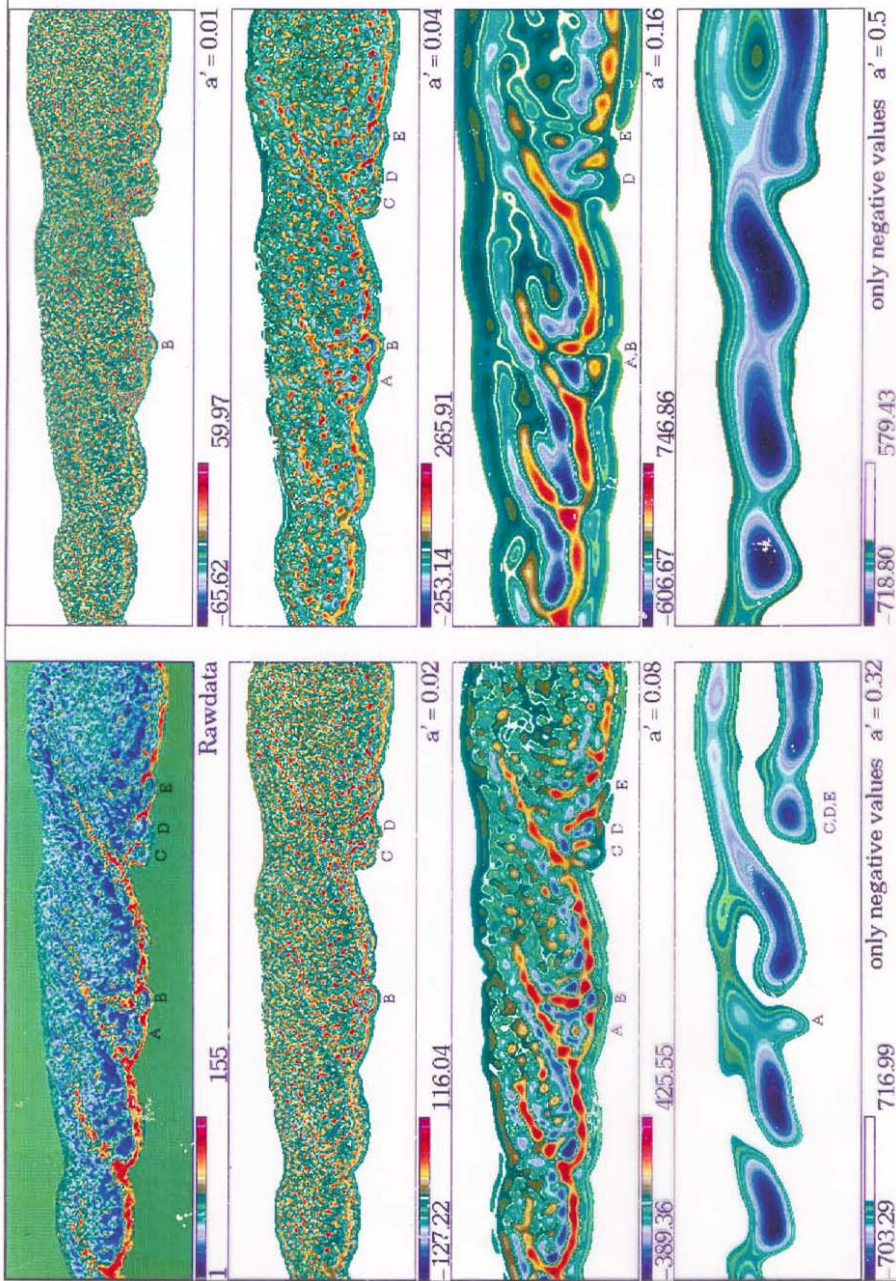
Figure 2. Wavelet transforms of the turbulent mixing layer (after Kailas & Narasimha 1999). *Top left:* raw image; rest are contoured wavelet transforms at the scales noted.
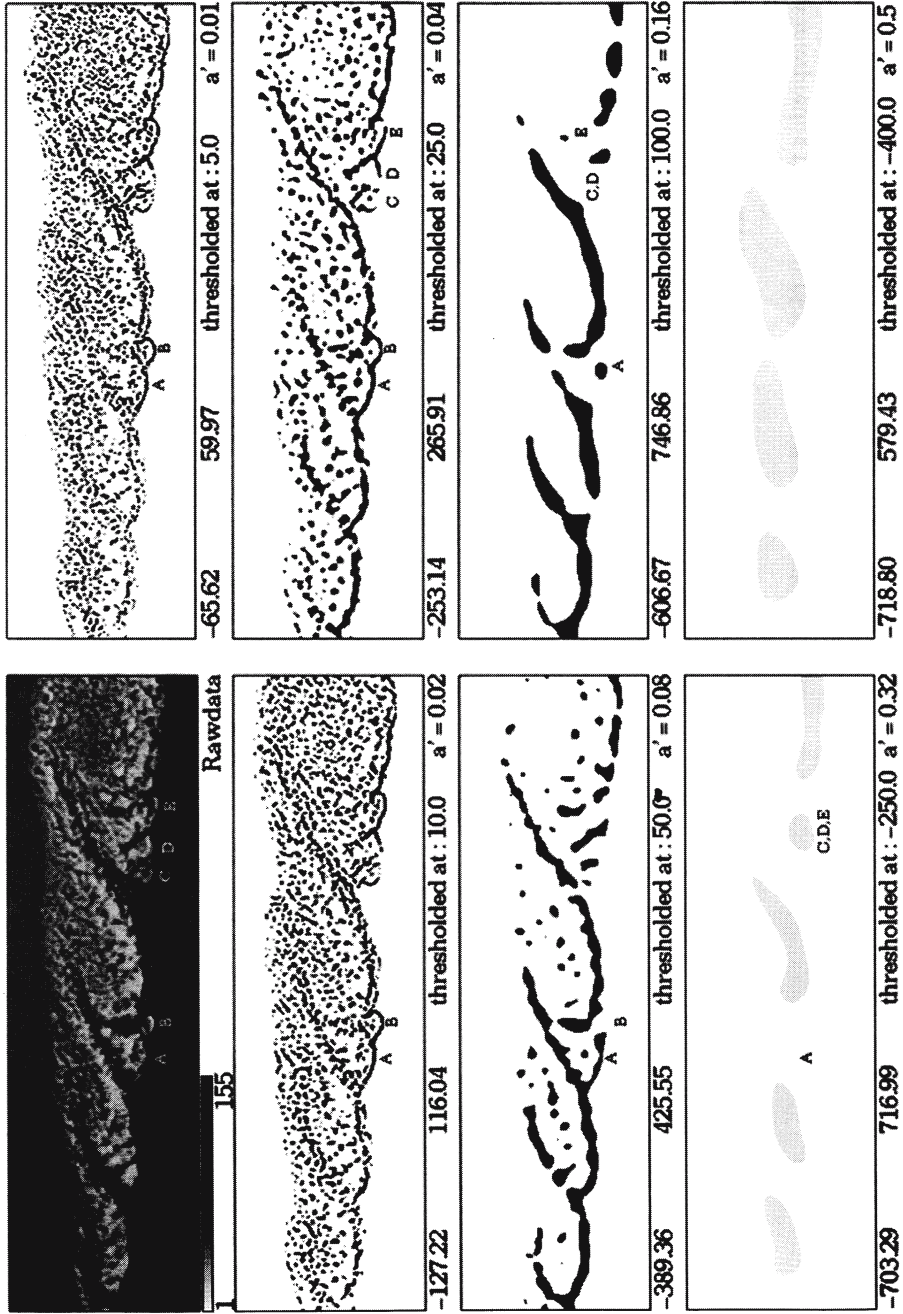
Figure 3. Structures detected in the mixing layer of figure 2, thresholded at appropriate levels at each scale as shown on the relevant panel (from Kailas & Narasimha 1999).

a' greater than 0·04 (and particularly at $a' = 0·16$) the edges of the large scale vortices, so conspicuous in the original (unprocessed) pictures, show clear elongated structures that appear to be cross sections of thick rolled-up sheets. At $a' = 0·08$, the vortex core is occupied by structures bigger in size than those seen at the smallest scales, but these too do not exhibit any strong variability in size with x.

The 'breaking wave' picture of the mixing layer is already revealed at $a' = 0·04$; at $a' = 0·08$, the analogy is particularly strong. The lower arms of the vortices are seen as distinct regions that rise along the edge of a vortex and appear to break up at the top and into the core.

The simplest method of detecting structures from the wavelet-transformed images is to study them at different thresholds. The optimum threshold reveals the structures captured unique to that scale without unnecessary clutter. Figure 3 shows the results, along with the thresholds adopted. At the lowest wavelet scales ($a' = 0·01$, 0·02 and even 0·04), the relatively homogeneous distribution of the small scale structure is again clearly seen. Based on the significant intermittency (with rapid fluctuations between values corresponding to the pure fluid on either side of the mixing layer) seen in point measurements of passive transportable scalars in a mixing layer, Roshko (1976) had concluded that distinctly separate small scale structures are embedded within the large scale vortices. The present analysis is consistent with this picture, but additionally reveals that these are relatively homogeneously distributed.

Now the wavelet results on the small scale structure may be explained by the dependence of the Kolmogorov length scale l_* on downstream distance in different flows. It is well known that $l_* \sim \varepsilon^{-1/4}$, where ε is the specific dissipation, proportional to U^3/δ, where U and δ are characteristic large-eddy velocity and length scales. Using the standard similarity laws, it is easily seen that $l_* \approx x^{1/4}$ in a mixing layer and $l_* \approx x$ in a round jet: the small scales are much less sensitive to downstream distance in a mixing layer compared to a jet. It is gratifying that the low-scale wavelets are able to capture these distinct properties of the mixing layer and jet flows.

In summary, three levels of scale-specific structures are revealed in the turbulent mixing layer: the nearly homogeneously distributed small scale structure, an intermediate scale organisation of the vortex boundaries (with some internal sub-structures), and the large-scale coherence of each vortex itself. While the latter two structure types are discernible in the raw image, the result on the smallest scale structures is not similarly evident.

5. Jets and plumes

The other class of flows where we have extensively used wavelet techniques is that of jets and plumes.

Over the last decade, a series of experimental and numerical studies have been carried out on the effect of appreciable quantities of off-source volumetric heating on the development of turbulent jets and plumes (Bhat & Narasimha 1996; Venkatakrishnan *et al* 1998, 1999; Basu & Narasimha 1999; see Narasimha & Bhat 2007 for a recent review). The motivation for the studies has been both technological (e.g. combustion) and meteorological; in particular, the effect of release of latent heat into the flow, following condensation of water vapour, on the fluid dynamics of the cloud was successfully simulated in the laboratory (see figure 4, for example). Indeed, the quest for an explanation of their unusual entrainment characteristics led to the development of some of the wavelet techniques developed here. In such flows, the entrainment of ambient fluid by cumulus clouds has been of great interest. A variety of earlier studies explored the issue of entrainment (for example, Morton *et al* 1956; Turner 1973, 1986; see Bhat & Narasimha 1996 for a discussion). In general, these early models predicted that
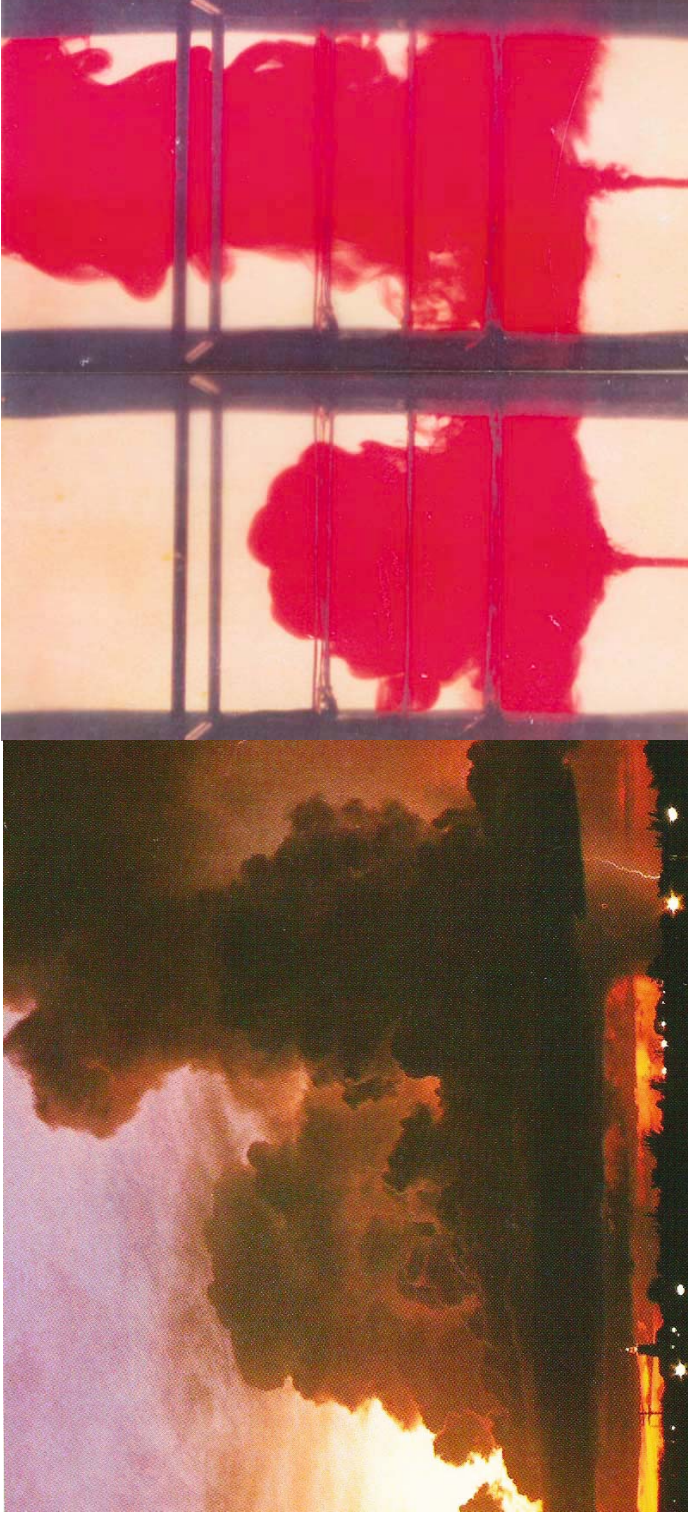
Figure 4. (**a**) Natural clouds. (**b**) Image from a dye-flow visualization of a jet subjected to off-source volumetric heating (see also figure 5a), neutral with respect to ambient in the lower, denser layer below where the jet spreads out horizontally (after Narasimha & Bhat 2007).
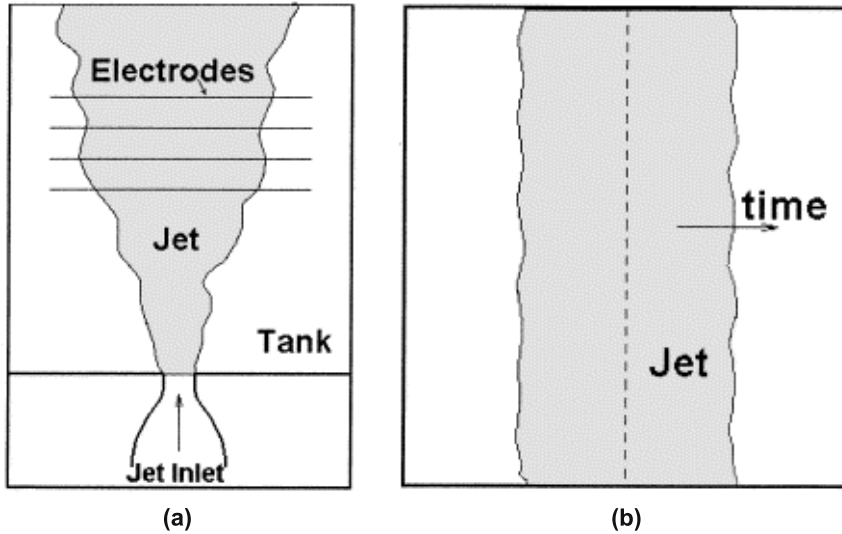
Image created by Narasimha, Bhat, Nagarathna

Figure 5. **(a)** Schematic of the experimental arrangement in a jet subjected to off-source heating through a series of electrodes. **(b)** Temporal simulation of the flow shown in (a); the method used is spectral, with periodic boundary conditions on the sides of the box.

when buoyancy is enhanced at and beyond a certain station in the flow, as happens in the case of clouds consequent to the release of the latent heat of condensation, the entrainment increases. However, all the evidence of cumulus clouds suggests that there is proportionately less entrainment than such predictions indicate. It is a matter of common observation that a cloud does not spread laterally in the way that turbulent shear flows normally do.

Experiments conducted by Bhat & Narasimha (1996) (figure 5a) showed that heat addition actually reduces the entrainment coefficient defined by Turner (1973). On the basis of the laser flow visualization pictures taken in this flow, they attributed the observed dramatic effect on entrainment in flows with heat addition to the disruption of the coherent structures present in the unheated flow.

First consider the classical round jet. We carry out a wavelet analysis of planar laser-induced fluorescence (PLIF) images of diametral sections of the jet. With one such image taken from the work of Venkatakrishnan *et al* (1999), Narasimha *et al* (2002) examined wavelet transforms at various scales, as with the mixing layer of §4. As expected, the transforms at the lower wavelet scales reveal the small scale structure of the turbulence. At larger scales, however, e.g. at $a' = 0.80$ (figure 6), a sinuous or fluted ring-like structure of the unheated plume is clearly seen, with a void inside and a green outer band. The ring is not completely axisymmetric, but has five (or possibly six) lobes. These lobes are reminiscent of the 'cells' that Basu & Narasimha (1999) reported in the vorticity field in a cross section of the jet, for which they provided direct numerical simulation (DNS) results. (The DNS solves the incompressible Navier–Stokes equations under the Boussinesq approximation for the temporal evolution of a jet-like flow, see figure 5b.)

To interpret the ordered structure of figure 6, it is useful to examine the DNS results, which have the advantage that any flow variable is accessible from the solution. Particular interest attaches to the vorticity vector and its components (azimuthal, radial and streamwise). Siddhartha *et al* (2000) have made a wavelet analysis of the vorticity field. They find that
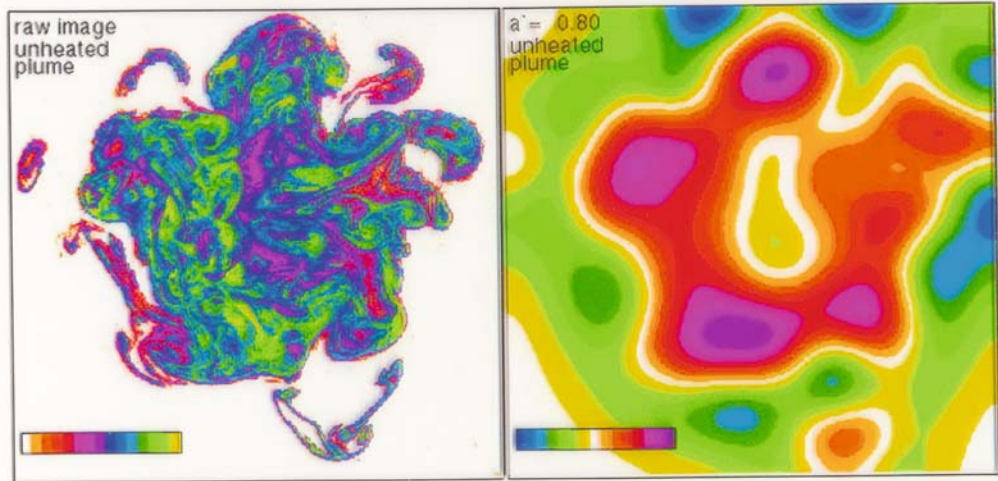
Figure 6.   *Left*: PLIF image of a section of a plume at 79·4 diameters from the orifice on the floor of the tank (Venkatakrishnan *et al* 1998). *Right*: Colour-coded contour intervals of the wavelet transform coefficient of the image on the left at a scale $a' = 0·8$ (Narasimha *et al* 2002).

the nature of the coherent motion is most strongly evident in the azimuthal component of the vorticity, which is organized in the form of a toroidal base supporting a relatively thin conical sheath; the interior of the structure is nearly devoid of azimuthal vorticity. There is some evidence of a secondary structure in the radial and streamwise components of the vorticity, which show strips of opposite sign close to each other, suggesting vortex pairs, possibly helically organized.

Let us return to the question of the 'lobes' (usually five or six) in the wavelet images at larger scales, especially in the ring regime of figure 6. By comparison with the analysis of the DNS results for the azimuthal vorticity by Siddhartha *et al* it seems plausible that the ring we see in the wavelet analysis of the experiments represents a vortex. It is then tempting to attribute the observed lobes to the well-known Widnall instability. Srinivas *et al* (2007) examine this question in the light of the theory of Widnall & Tsai (1977), according to whom a vortex ring always exhibits a bending instability for at least the lowest two critical azimuthal wave numbers. Estimating the radius of the vortex ring and its core from the DNS, Srinivas *et al* (2007) find that the number of lobes predicted by the Widnall theory can be anywhere between 3 and 11, depending on the precise dimensions of the ring. The observed range of five to six lobes lies in the middle of the predicted range, and, given the uncertainties in estimating the observed ring dimensions, they conclude that the observed number of lobes is not inconsistent with a form of the Widnall instability.

Srinivas *et al* (2007) process a large number of images by the techniques described above, and by stacking them in time can produce movies of the transformed image at any wavelet scale. From such wavelet movies they can construct the life cycle of a coherent structure as it passes through the plane of observation illuminated by the laser sheet. Thus, by analysing the amount of ambient fluid in the core of the jet, they find a quasi-cyclic behaviour with an average period T given by $U_c T/b$ of about 6, where U_c is the centre-line velocity in the jet and b is its half-width. This period is also the average time taken by a coherent structure to pass the section of observation.
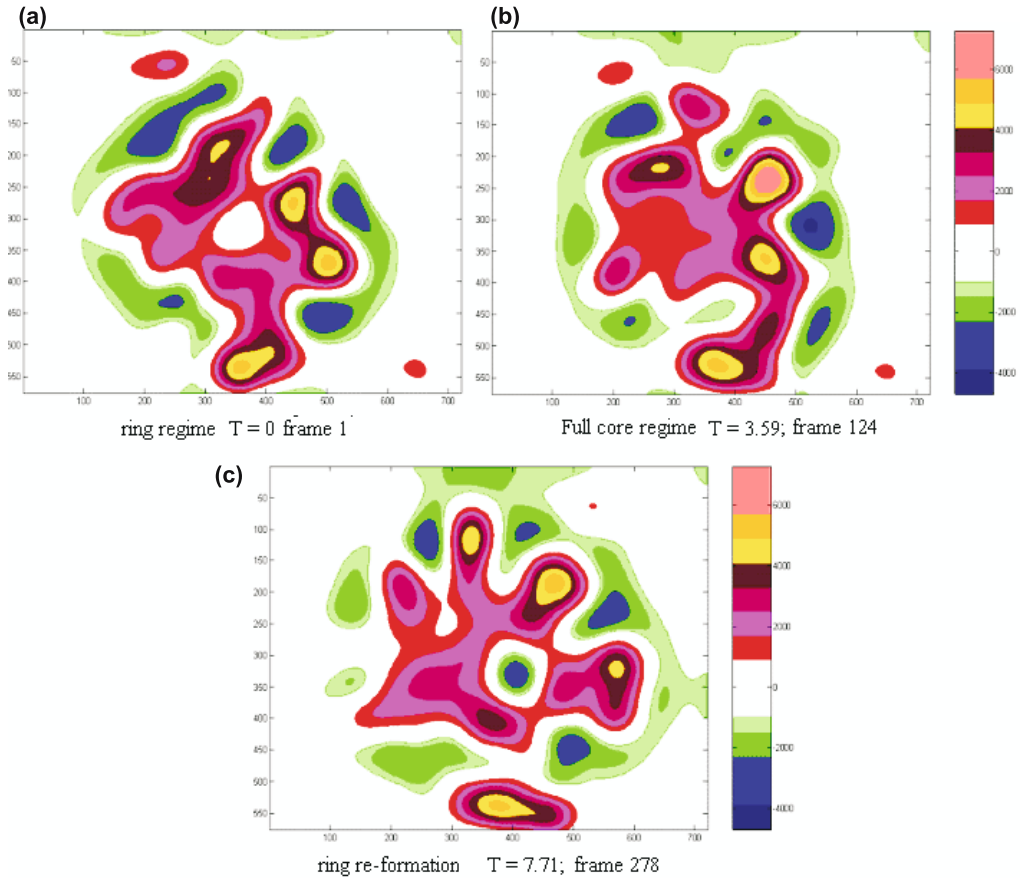
Figure 7. Wavelet transform images through one complete quasi-cycle as one coherent structure passes the plane of observation. **(a)** Ring regime, **(b)** full-core regime, **(c)** return to ring image (Srinivas *et al* 2007).

Such a cycle (figure 7), or more precisely a quasi-cycle, is marked by the presence of three distinct regimes respectively, representing a ring regime, a dye-filled core regime, and an intermediate mixed regime. Each of the first two regimes occupies about 8% of the time in a cycle, the mixed regime prevailing over the rest of the time.

A wavelet movie of the same kind has not yet been produced for the heated jet, but selected 'stills' have been processed. We show the effect of off-source heating on the jet through one such still in figure 8. By comparison with figure 6 we can see how the coherence and order seen in the unheated flow is disrupted by heating. Heating accelerates the flow. Also, the baroclinic torque resulting from the heating enhances the vorticity dramatically Basu & Narasimha 1999. The coherent structures, as a result, get stretched streamwise and run into their downstream counterparts. After prolonged heating, this leads to a complete breakdown of coherent motion. It is the disruption of the structure seen in figure 6 to the dye-filled regime of figure 8 that has been proposed as the mechanism responsible for the drastic alteration of the entrainment characteristics by Bhat & Narasimha (1996). In fact, the possibility of using heat to control entrainment in jets has been discussed by Narasimha & Sivakumar (1999).
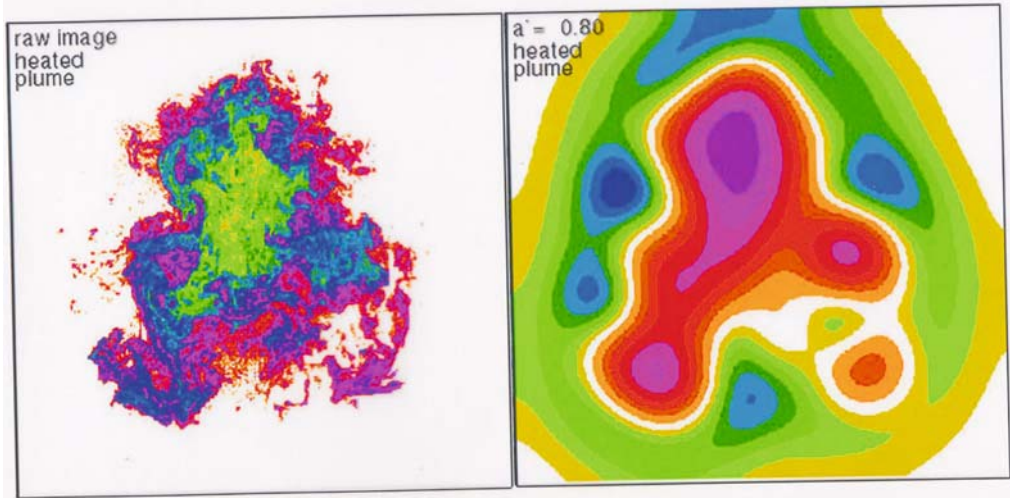
Figure 8. *Left*: PLIF image of a diametral section of a plume with off-source heating of 555 W (Venkatakrishnan *et al* 1998). *Right*: Colour-coded contour intervals of the wavelet transform coefficient at a scale $a' = 0.8$ (Narasimha *et al* 2002).

6. Conclusion

The work briefly reviewed here shows that wavelet processing of flow-visualization imagery provides us with a powerful tool for studying the structure and life-cycle of coherent structures in turbulent shear flows. This power has been illustrated by analysing, for the first time, a sequence of images of diametral sections of a turbulent jet through the dye-concentration fields provided by the laser-induced fluorescence technique. The analysis helps us to describe the life cycle of a coherent structure as it passes through the test section.

When experimental data can be combined with DNS results, wavelet analysis of both provides us with considerably more insight than either of them can do by itself. In the case of jets, this approach leads to the proposal that the ring observed in wavelet images here may represent the vortex at the base of the arrowhead-shaped coherent structure that characterizes the turbulent jet. Furthermore, the number of lobes that are so clearly seen in the wavelet imagery at the larger scales is roughly consistent with the predictions made by the theory of instability of vortex rings due to Widnall and her co-workers.

These results pertain to a jet Reynolds number of 2280, and cannot be automatically expected to hold at much higher Reynolds numbers, which still need to be investigated. The probability of finding pure ambient fluid at the centre of the jet decreases as the jet Reynolds number increases, but as structures are known to persist to very high Reynolds numbers, it is conceivable that a ring of higher concentration still surrounds a fluid of lower (although not zero) concentration in an appropriate ring regime even at high Reynolds numbers.

Thus wavelet techniques applied on flow imagery, derived from experiment and computation, provide powerful insights into the structure and evolution of coherent structures in turbulent shear flows. Further development of the techniques applied here seems worthwhile, as they have the potential to provide a new and effective diagnostic for identifying coherent structure characteristics in near-real time, with promising applications to flow control.

References

Addison P S 2002 *The illustrated wavelet transform handbook* (Bristol: Institute of Physics)

Arneodo A, Bacry E, Graves P V, Muzy J F 1996 Characterizing long-range correlations in DNA sequences from wavelet analysis. *Phy. Rev. Lett.* 74: 3293–3296

Azad S, Narasimha R 2007 Multi-resolution analysis for separating closely spaced frequencies with an application to Indian monsoon rainfall data. *Int. J. Wavelets, Multi Resolution Inf. Process.* (to appear)

Basu A J, Narasimha R 1999 Direct numerical simulation of turbulent flows with cloud-like off-source heating. *J. Fluid Mech.* 385: 199–228

Bhat G S, Narasimha R 1996 A volumetrically heated jet: large-eddy structure and entrainment characteristics. *J. Fluid Mech.* 325: 303–330

Brown G L, Roshko A 1974 On density effects and large structures in turbulent mixing layers. *J. Fluid Mech.* 64: 775–816

Cutler A D, Johnson C H 1997 Analysis of intermittency and probe data in supersonic flow with injection. *Exp. Fluids* 23: 38–47

Everson R, Sirovich L, Sreenivasan K R 1990 Wavelet analysis of the turbulent jet. *Phys. Lett.* A145: 314–322

Farge M 1992 Wavelet transforms and their applications to turbulence. *Annu. Rev. Fluid Mech.* 24: 395–457

Fiedler H E 1988 Coherent structures in turbulent flows. *Prog. Aero. Sci.* 25: 231–270

Hussain A K M F 1986 Coherent structures and turbulence. *J. Fluid Mech.* 173: 303–356

Kailas S V, Narasimha R 1999 The eduction of structures from flow imagery using wavelets. Part I. The mixing layer. *Exp. Fluids* 27: 167–174

Kline S J, Reynolds W C, Schraub F A, Runstadler P W 1967 Structure of turbulent boundary layers. *J. Fluid Mech.* 30: 741–773

Marr D 1982 *Vision* (New York: Freeman)

Meier G E A, Viswanath P R (eds) 1999 Mechanics of passive and active flow control. *Proc. IUTAM Symposium* (Dordrecht: Kluwer)

Meyer Y 1993 *Wavelets: Algorithms and applications* (Philadelphia: SIAM)

Morton B R, Taylor G I, Turner J S 1956 Turbulent gravitational convection from maintained and gravitational sources. *Proc. R. Soc.* A234: 1–23

Narasimha R, Sivakumar I V R 1999 Manipulating coherent structures by heat in a Boussinesq jet. In: Meier & Viswanath (1999) pp 209–216

Narasimha R, Saxena V, Kailas S V 2002 Coherent structures in plumes with and without off-source heating using wavelet analysis of flow imagery. *Exp. Fluids* 33: 196–201

Narasimha R, Bhat G S 2007 Recent experimental and computational studies related to the fluid dynamics of clouds. *Proc. IUTAM Symp. Computational Physics and New Perspectives in Turbulence*, Nagoya, 11–14 Sep. 2006 (to be published)

Roshko A 1976 Structure of turbulent shear flows: a new look. *AIAA J.* 44: 1349–1357

Siddhartha S S, Narasimha R, Basu A J, Kailas S V 2000 Coherent structures in numerically simulated jets with and without off-source heating. *Fluid Dyn. Res.* 26: 105–117

Srinivas A, Bhat G S, Narasimha R 2007 Dynamic eduction of coherent structures in turbulent jet flow imagery by wavelet techniques: Part I. *J. Turbulence* 8: 1–14

Strang G 1989 Wavelets and dilation equations: A brief introduction. *SIAM Rev.* 31: 614–627

Townsend A A 1976 *The structure of turbulent shear flow* 2nd edn (Cambridge: Cambridge University Press)

Tso J, Hussain F 1989 Organised motions in a fully developed turbulent aaxisymmetric jet. *J. Fluid Mech.* 203: 425–448

Turner J S 1973 *Bouyancy effects in fluids* (Cambridge: University Press)

Turner J S 1986 Turbulent entrainment: the development of entrainment assumption and its application to geophysical flows. *J. Fluid Mech.* 173: 431–471

Venkatakrishnan L, Bhat G S, Prabhu A, Narasimha R 1999 Experiments on a plume with off-source heating: Implications for cloud fluid dynamics. *J. Geophys. Res.* 104: 14,271–14,281

Venkatakrishnan L, Bhat G S, Prabhu A, Narasimha R 1998 Visualization studies of cloud-like flows. *Curr. Sci.* 74: 597–606

Widnall S A, Tsai C Y 1977 The instability of the thin vortex ring of constant vorticity. *Philos. Trans. R. Soc.* A287: 273–305